This is the accepted version of the following article:

Xiaodong Ji, Xiaowei Cheng, Xiangfu Jiang, Amit H. Varma. Cyclic shear behavior of double-skin composite walls for high-rise buildings. Journal of Structural Engineering (ASCE), 2017, 143(6): 04017025.

which has been published in final form at [Link to final article].

Cyclic In-Plane Shear Behavior of Double Skin Composite (DSC) Walls in High-Rise Buildings

Xiaodong Ji[1], Xiaowei Cheng[2], Xiangfu Jia[3], Amit H. Varma[4]

[1]Associate professor, Key Laboratory of Civil Engineering Safety and Durability of China Education Ministry, Department of Civil Engineering, Tsinghua University, Beijing 100084, China

[2]Graduate student, Beijing Engineering Research Center of Steel and Concrete Composite Structures, Department of Civil Engineering, Tsinghua University, Beijing 100084, China

[3]Graduate student, Department of Civil Engineering, Tsinghua University, Beijing 100084, China

[4]Professor, Lyles School of Civil Engineering, Purdue University, West Lafayette, IN 47907, M. ASCE

Abstract: Double skin composite (DSC) walls consist of a thick concrete infill sandwiched in between two steel faceplates on the exterior surfaces. DSC walls used in high-rise buildings have higher reinforcement ratios, and are subjected to larger axial force ratios as compared to DSC walls used in safety-related nuclear facilities. This paper presents the results of experimental and numerical investigations conducted to evaluate the cyclic in-plane shear behavior of DSC walls for high-rise buildings, and the influence of higher reinforcement ratios and axial force ratios. The DSC wall specimens were designed with a reinforcement ratio of 6.4%, and with flange walls designed as boundary elements to ensure that the walls would be shear critical. The wall specimens failed by cyclic yielding and local buckling of the steel faceplates in the web walls, and eventual crushing of the concrete infill. The steel

Please cite this article as: Xiaodong Ji, Xiaowei Cheng, Xiangfu Jiang, Amit H. Varma. Cyclic shear behavior of double-skin composite walls for high-rise buildings. Journal of Structural Engineering (ASCE), 2017, 143(6): 04017025. DOI: 10.1061/(ASCE)ST.1943-541X.0001749.

faceplates prevented spalling of the crushed concrete, and as a result, the wall specimens had stable hysteretic loops and large shear deformation capacity. Using vertical stiffeners and tie plates as connectors further increased the shear deformation capacity of the wall specimens, with the ultimate shear strain reaching 3%. A mechanics based model (MBM), developed previously by Varma et al. (2014), was used to analyze the in-plane shear response of the wall specimens. The experimental and analytical investigations indicate that axial compression has limited influence on the shear strength, but decreases the shear deformation capacity of the DSC walls. Analytical parametric studies indicate that for DSC walls made using normal strength concrete and steel, high reinforcement ratios (of over 7.5%) and high axial force ratios (exceeding 0.40) can potentially lead to crushing of the concrete infill prior to yielding of steel faceplates, and thus non-ductile failure modes. Finally, the design equations specified in various codes are verified using experimental results of 42 specimens from past tests and from this experimental program. JEAC-4618 2009 (Japan), KEPIC-SNG 2010 (S. Korea), AISC N690s1-15 (U.S.) and JGJ 3-2010 (China) code equations provide reasonable and conservative estimations of the shear strength of DSC walls, with the ratio of experimental-to-calculated values equal to approximately 1.30 on average.

Keywords： Double skin composite walls; Steel-plate Composite Walls; Composite Construction; Cyclic shear behavior; Shear strength; Mechanics based model; Deformation capacity; Design equations

Introduction

Double skin composite (DSC) walls, also referred as steel-plate composite (SC) walls, are composed of a thick concrete infill sandwiched in between two steel faceplates on the exterior surfaces. The steel faceplates are anchored to the concrete infill using steel headed studs (shear studs), and the opposite faceplates are connected to each other using tie bars through the concrete infill. The steel faceplates serve as primary reinforcement for the concrete infill to resist in-plane membrane forces and out-of-plane moments (Varma et al. 2014). The tie bars also serve as out-of-plane shear reinforcement for the concrete infill to resist out-of-plane shear forces (Sener and Varma 2014). The shear studs and tie bars develop composite action between the steel faceplates and the concrete infill by resisting the interfacial shear forces (Zhang et al. 2014). The steel faceplates prevent spalling of concrete infill, while the shear studs and concrete infill enhance the stability of the steel faceplates (Zhang et al. 2014). This synergistic interaction between the steel and concrete components of DSC walls enhances their seismic performance (Varma et al. 2011).

The steel modules consisting of the faceplates, shear studs and tie bars can be pre-fabricated in the shop and shipped to the field for erection and concrete placement, thus expediting construction and improving quality control. The steel faceplates also serve as permanent stay-in-place formwork for casting concrete, which can potentially improve construction efficiency over conventional reinforced concrete (RC) walls. Due to these potential advantages, DSC walls have been used extensively in modern safety-related nuclear facilities (Varma et al. 2014, AISC N690s1 2015) and other infrastructure (Liew et al, 2015). More recently, DSC walls have been of significant interest in high-rise buildings (e.g., Ding et al. 2011; Bruneau et al. 2016). The use of such composite walls can reduce the thickness of walls, resulting in more efficient use of space and reduced gravity loads. Fig. 1 shows a photograph of on-site construction of DSC walls for a television tower in Yancheng, China.

Since the early 1990s, extensive experimental tests and analysis have been conducted to evaluate the behavior of DSC walls to various in-plane, out-of-plane, and combined loading conditions (e.g., Akiyama et al. 1991, Takeda et al. 1995, Takeuchi et al. 1998, Ozaki et al. 2004, Varma et al. 2011, Sener and Varma 2014, Varma et al. 2014, Zhang et al. 2014, Seo et al. 2016, and Kurt et al. 2016). These studies form a valuable database of test results for DSC walls. However, these tests focus on walls used in safety-related nuclear facilities, which have steel reinforcement ratio (defined as $2t_p/T$), ranging from 1.5 to 5% (Varma et al. 2014), where t_p denotes the steel faceplate thickness and T denotes the wall thickness. In addition, those walls are subjected to relatively low axial force ratios, which is different from the situation for DSC walls used in lower stories of high-rise buildings.

Recently, there has been great interest in the design and use of DSC walls in high-rise buildings (e.g., Eom et al. 2009, Ji et al. 2013, Nie et al. 2013, Alzeni and Bruneau 2014, Bruneau et al., 2016). In high-rise buildings, these DSC wall will have higher reinforcement ratios and may be subjected to larger axial force ratios. Most of these recent studies focus on the in-plane flexural behavior of slender DSC walls, and experimental data focusing on the cyclic in-plane shear behavior of DSC walls in high-rise building is limited. Increasing the axial force may influence the in-plane shear strength of walls, expedite crushing of the concrete infill, and consequently decrease the deformation capacity of the walls.

The objective of this study is to investigate the cyclic in-plane shear behavior of DSC walls used in high-rise buildings, and to evaluate the influence of increased reinforcement ratios and axial force ratios on the shear behavior of DSC walls. This paper presents the results from a series of quasi-static cyclic tests conducted to evaluate the shear behavior of DSC walls under moderate to high axial force ratios. Furthermore, a mechanics based model (MBM), developed previously by Varma et al. 2014, is used to calculate the in-plane shear behavior and strength of the wall specimens, and to discuss the effects of axial force ratio and steel reinforcement ratio on in-plane shear behavior. Finally, the paper evaluates the design equations provided in international design codes for calculating the nominal in-plane shear strength of DSC walls. The code equations are evaluated by using them to predict the shear strength of DSC walls in a large database assembled by the authors. This database included results from specimens with a wide range of reinforcement ratios and axial force ratios.

Experimental Program

Test specimens

The test specimens were designed to represent the lower stories of structural walls in a 150-m tall building, and were fabricated at approximately 1/3-scale to accommodate the capacity of the loading facility. A total of three wall specimens (labeled as DSCW1 through DSCW3) were designed and fabricated. The testing concept in this paper is similar to Varma et al. (2011) and Seo et al. (2016), where the wall specimen was designed with flanges to enforce pure in-plane shear behavior and failure in the web wall. The DSC web wall primarily resists in-plane shear, while the two flange walls resist the overturning moment. The in-plane flexural strength of the overall wall specimen was designed to be greater than 1.5 times its in-plane shear strength. The flexural strength of the DSC wall was assessed using the program XTRACT for cross-section analysis, while the shear strength was calculated using the JGJ 3-2010 equations that will be presented later.

Fig. 2 shows the overall geometry, structural layout, and reinforcement details for Specimens DSCW1 and DSCW2. The two specimens were identical, except for the applied axial compressive load. As shown in Fig. 2(a), the clear height of the wall specimen above the foundation was 0.85 m. The specimens were cast integrally with the foundation beam (0.8 ×0.8×2.6 m in size) and loading beam (0.35×0.35×1.0 m in size). The foundation beam was designed with large dimensions and heavy reinforcement to ensure that it was damage free during testing. As shown in Fig. 2(b), the clear length of the web wall was 0.61 m, and the thickness of the flange walls was 0.12 m. The thickness of the web wall was also 0.12 m, and the length of flange walls was equal to 0.52 m. As shown in Fig. 2(a), the flange walls were intentionally disconnected from the top beam to limit the possible shear contribution induced by the secondary bending moments of the flange walls and for easy installation of loading threaded bars (Ji et al., 2015).

The DSC web wall had faceplate thickness, t_p, equal to 4 mm for all specimens. The steel reinforcement ratio, $2t_p/T$, of the DSC web wall was equal to 6.4%, where T denotes the thickness (0.12m) of web wall. DSC walls used for high-rise buildings have steel reinforcement ratios ranging from 6% to 8%, which is larger than the values (1.5-5%) recommended for walls in safety-related nuclear facilities (Varma et al. 2014).

Specimens DSCW1 and DSCW2 used a typical combination of shear studs and tie bars, as shown in Fig 2(b), to develop composite action between steel faceplates and concrete infill, and to prevent local buckling of steel faceplates. Tie bars provide composite action as well, but are used most importantly to provide structural integrity by connecting the two faceplates to each other through the infill. Table 1 presents the details of the connections. The headed shear studs were designed to satisfy the design criteria proposed by Zhang et al. (2014). The faceplate slenderness ratio (i.e., the ratio of the stud spacing s over the steel faceplate thickness t_p) was equal to 25, which satisfies the AISC N690s1-15 slenderness limit of $1.0\sqrt{E/f_y}$ for non-slender steel faceplates to prevent local buckling before yielding.

As the web wall sustained in-plane shear only, the design of tie bars did not consider the requirement for out-of-plane shear reinforcement. Tie bars were designed to ensure that the out-of-plane deformation of faceplates were minimal under the hydrostatic pressure during pouring concrete. The DSC flange walls were designed to resist the overturning moment developed at the wall bases. The steel faceplates of the DSC flange walls were intentionally thickened to 8 mm to ensure large flexural strength of the overall wall specimen. The web faceplates were welded to the flange faceplates using complete-joint-penetration (CJP) groove welds. As shown in Fig. 2(b) and (c), U-shaped rebars were used to provide the bond shear strength along the interface between the steel plate of the flange wall and the concrete infill of the web wall by the shear-friction mechanism (Shirali 2002, Ji et al. 2013). The U-shaped rebars were connected with the steel plate of the flange wall using fillet welds, and the fillet weld was designed to be stronger than the tensile strength of the U-shaped rebars.

Specimen DSCW3 was identical to Specimens DSCW1 and DSCW2, with the exception that it used a novel connector for developing composite action and for tying the faceplates together, as shown in Fig 3. Vertical stiffeners were welded to the faceplates using fillet welds and they were connected to each other using tie plates (Nie et al. 2013). The ratio of the stiffener spacing (s) over the steel faceplate thickness (t_p) was 37.5, which is greater than the AISC N690s1-15 slenderness limit, but less than the limiting width-to-thickness ratio of $1.4\sqrt{E/f_y}$ for highly-ductile rectangular filled composite members specified by AISC 341-10.

Fig. 2(c) and 3(b) shows the elevation view of the specimen. All steel plates were securely anchored to the foundation beams. The DSC web wall faceplates were extended into the top beam, but the faceplates of DSC flange walls were disconnected from the top beam as explained earlier.

The strength grade of the concrete infill in all wall specimens was C50, with the nominal cube compressive strength f_{cu} equal to 50 MPa. Three cubes of 150 mm in size were tested on the day of specimen testing. The average value of the measured cube compressive strength $f_{cu,t}$ was equal to 47.6, 52.7 and 50.5 MPa for Specimens DSCW1 through DSCW3, respectively. The axial compressive strength of the concrete was taken as $f_{c,t}$ = $0.76f_{cu,t}$ according to the Chinese code for design of concrete structures GB 50010-2010.

All the steel plates used for the DSC specimens had a strength grade of Q235 (the nominal yield strength f_y = 235 MPa). Table 2 summarizes the properties of the steel, which are the average values obtained from standard coupon tests. Three coupon specimens were tested for each type of steel. The U-shaped rebars were deformed bars, and their strength grade was HRB400 (f_y = 400 MPa). The yield and ultimate strengths measured using coupon tests were equal to 424 and 636 MPa, respectively. The measured yield and ultimate strengths of D8 (diameter = 8 mm) shear studs were equal to 363 and 444 MPa, respectively. D8 tie bars had a strength grade of 8.8 (nominal ultimate strength f_u = 800 MPa, and the ratio f_y/f_u = 0.8). Their measured yield and ultimate strengths were equal to 634 and 816 MPa, respectively.

Axial force ratio

In accordance with the Chinese technical specification for concrete structures of tall building JGJ 3-2010, the axial force ratio for composite walls can be calculated using Eq. (1).

$$n = \frac{N}{f_c A_c + \sum f_y A_s} \tag{1}$$

where, N denotes the axial force applied to the wall, f_c denotes the axial compressive strength of the concrete, f_y denotes the yield strength of steel plates, and A_c and A_s denote the cross-sectional areas of concrete infill and steel plates, respectively.

As the flange walls of the specimens were disconnected from the top beam, the axial force was applied primarily to the DSC web wall in the upper portion of the specimen. However, the axial force could spread and transfer to the flange walls in the lower portion of the specimen. This spreading of the axial force was evaluated nominally by preliminary finite element analysis. An elastic finite element model was developed using solid elements to represent the DSC wall specimen. The model included the boundary and loading conditions of the tested specimens. The analysis results indicated that the DSC web wall resisted an average of approximately 77% of the applied axial force. The axial force ratio for the DSC web walls was calculated using Eq. (1), the approximate proportion (77%) of the applied axial force, the measured dimensions of the DSC web wall, and the actual strength of steel and concrete materials. Specimen DSCW1 had a moderate axial force ratio of 0.16, while Specimens DSCW2 and DSCW3 had a high axial force ratio of 0.31.

Test setup and instrumentation

Fig. 4 shows the test setup. The axial force was first applied and maintained constant during the test. The lateral cyclic loading was applied in displacement-control using two actuators. The first three cycles were applied in the elastic range of response, i.e., before yielding or inelasticity in the specimen. Three levels of drifts were included, i.e. 0.05%, 0.1% and 0.2%, and one cycle was performed at each level. After the specimen reached the estimated yield drift of 0.4%, the lateral displacement was increased with increments of 0.4% drift, and two cycles were repeated at each drift level. The test was terminated when the specimen failed completely due to crushing of the concrete infill.

Instruments were used to measure loads, displacements and strains in the specimen. Load cells measured the vertical and lateral loads applied to the specimen. Fig. 4(a) shows the layout of linear variable differential transformers (LVDTs) mounted to the specimens. LVDT d1 measured the lateral displacement at the centroid of the top beam, which was used for the displacement control of the lateral loading. LVDT d2 measured the lateral displacement at the wall top. A pair of diagonal LVDTs (i.e., d3 and d4) measured the shear deformation of the web wall. Four LVDTs (i.e., d5 through d8) were mounted along both wall edges to measure the flexural deformation of the wall. LVDTs d9 and d10 were used to monitor any rotation of the foundation beam, and LVDT d11 was used to monitor slip of the foundation beam along the reaction floor. Nine sets of strain-gauge rosettes were mounted to the steel faceplates, and their location is shown in Fig. 8. Strain gauges were used to measure the vertical strains in the flange faceplates at the wall base. The strains in a few shear studs, tie bars, tie plates and U-shaped bars were also monitored.

Experimental results

Hysteretic responses

The in-plane shear deformation Δ_{sh} and average shear strain γ of the web wall were estimated using the data measured by diagonal LVDTs d3 and d4 as follows

$$\Delta_{sh} = (\delta_3 - \delta_4)\sqrt{a^2 + b^2} / 2ab \tag{2}$$

$$\gamma = \Delta_{sh} / b \tag{3}$$

where δ_3 and δ_4 denote the deformation measured by LVDTs d3 and d4, and a and b denote the clear length and height of the web wall as shown in Fig. 4.

Fig. 5 compares the lateral drift measured by LVDT d2 and the shear deformation measured by the diagonal LVDTs d3 and d4. While the total drift was dominated by the shear deformation, slight differences existed between those two values. The shear deformation Δ_{sh} and average shear strain γ measured by the diagonal LVDTs are used in the following discussion.

Fig. 6 shows the hysteresis loops of in-plane shear force versus the average shear strain calculated by Eqs. (2) and (3) using data measured by diagonal LVDTs. All the hysteresis loops were full, without obvious pinching even under large inelastic deformation. This is attributed to the fact that the steel faceplates had stable cyclic shear behavior and could prevent spalling of the concrete infill. Note that the hysteresis loops appear to be fuller than the test data of Varma et al. (2011) and Seo et al (2016), as the specimens in this paper had higher reinforcement ratio, and were subjected to larger deformation cycles. As Specimen DSCW2 was subjected to higher axial force, it showed a faster decrease of the post-peak strength relative to Specimen DSCW1. Specimen DSCW3, which used vertical stiffeners and tie plates for connecting two faceplates exhibited stable hysteretic loops up to very large shear strain of approximately 3%.

Damage and failure mode

Analysis of the data from the strain-gauge rosettes indicated the yielding of faceplates occurred at approximately 0.25% shear strain. Note that the principal strains were calculated from the strain-gauge rosette data, and then the elastic principal stresses were estimated from plane stress analysis using an assumed elastic modulus of steel E = 2.06 $\times 10^5$ MPa and poisson ratio ν = 0.3. The yielding of steel faceplates was assessed using the Von Mises criterion. Local buckling of faceplates was observed at 1.8% shear strain for Specimen DSCW1 and at 1.2% for Specimens DSCW2 and DSCW3. In the end, the concrete infill crushed at the location where the faceplates buckled. Fig. 7 shows the failure mode of the wall specimens, indicating that the local buckling of faceplates and damage was concentrated in the upper portion of the web wall where the axial force was larger than the lower portion.

Shear strength and deformation capacities

Table 3 summarizes the shear strength and deformation capacities of the specimens. The yield load V_y corresponds to the yielding of faceplates as measured by the strain-gauge rosettes. The yield shear strain γ_y is the average shear strain measured by diagonal LVDTs corresponding to the yield load V_y. The ultimate shear strain γ_u is defined as the post-peak shear strain corresponding to the lateral load that is 85% of the peak load. As Specimen DSCW3 did not show obvious strength degradation until complete failure, its ultimate shear strain was defined to be the maximum level of shear deformation sustained for at least one full cycle of loading prior to failure of the wall. The ductility factor is calculated as $\mu_\gamma = \gamma_u/\gamma_y$.

The following observations are made from Table 3. (1) All three specimens had similar yield shear strains, indicating that the axial force ratio had limited influence on the shear yielding of DSC walls. (2) The maximum shear strength of Specimens DSCW2 and DSCW3 with higher axial force ratio was approximately 5% larger than that of Specimen DSCW1, which had the lower axial force ratio. The axial force ratio appears to have limited influence on the shear strength capacity of DSC walls. (3) The ultimate shear strain of DSCW2 was 27% lower than DSCW1, indicating that the increase of axial force ratio leads to a decrease of shear deformation capacity in the DSC walls. (4) The vertical stiffeners and tie plates appeared to provide more effective restraint to the faceplates, and consequently DSCW3 had a significantly larger ultimate shear strain than other specimens.

Strains

Fig. 8 shows the principal strains and the corresponding directions measured by the strain-gage rosettes located on the faceplates at the yield point. The average angle between the principal tensile strain and horizontal direction was 37.4°, 35.3° and 29.6° for the web faceplates of Specimens DSCW1, DSCW2 and DSCW3, respectively. The reduction in the principal angle (corresponding to the principal tensile strain) at yield in Specimen DSCW2 and DSCW3 was caused potentially by the increased axial force ratio.

The strain gauge data also indicate that the faceplates at the flange wall base yielded slightly at large lateral drifts. The shear studs and U-shaped bars did not yield till the failure of the walls. Tie bars and tie plates sustained tensile yielding at 1.2% lateral drift.

Analysis of shear strength capacity

Mechanics based model (MBM)

Varma et al. (2011, 2014) developed a mechanics based model (MBM) used to predict the response of DSC walls subjected to in-plane shear forces. This model is based on the following assumptions: (i) isotropic elastic plane-stress behavior for the steel faceplates and the concrete infill before cracking, (ii) orthotropic elastic behavior of the concrete infill after cracking with zero stiffness in the principal tensile direction perpendicular to cracking, and reduced elastic stiffness for the principal compressive direction parallel to cracking, (iii) Von Mises yield criterion for the steel faceplates, and (iv) strain compatibility between the steel faceplates and concrete infill.

The DSC walls are assumed to be subjected to uniform membrane force (S_x, S_y, and S_{xy}) per unit length, resulting in the membrane averaged strains (ε_x, ε_y, γ_{xy}). Eq. (4) presents the relationship between the membrane forces and averaged strains for the composite walls. In this equation, T_c and T_s denote the thickness of the concrete infill and steel faceplates. $[K]_c$ and $[K]_s$ denote the stiffness matrices of the concrete infill and steel faceplate in global coordinate system, respectively, given by Eqs. (5) and (6). Note that $[K]_c = [K]_c^{uncr}$ before the concrete cracked, $[K]_c = [K]_c^{cr}$ after the concrete cracked. In Eq. (5), E_s and ν_s denote the elastic modulus and poisson ratio of the steel, E_c and ν_c denote the elastic modulus and poisson ratio for the uncracked concrete, E_c' denotes the reduced elastic modulus for cracked concrete and it is assumed to be 70% of the uncracked modulus E_c, and $[T]_\sigma$ and $[T]_\varepsilon$ denote the stress and strain transformation matrices.

$$\begin{bmatrix} S_x \\ S_y \\ S_{xy} \end{bmatrix} = \left\{ T_c [K]_c + T_s [K]_s \right\} \times \begin{bmatrix} \varepsilon_x \\ \varepsilon_y \\ \gamma_{xy} \end{bmatrix} \quad (4)$$

$$[K]_{\mathrm{s}} = \frac{E_{\mathrm{s}}}{1\text{-}\nu_{\mathrm{s}}^2}\begin{bmatrix} 1 & \nu_{\mathrm{s}} & 0 \\ \nu_{\mathrm{s}} & 1 & 0 \\ 0 & 0 & \dfrac{1\text{-}\nu_{\mathrm{s}}}{2} \end{bmatrix} \tag{5}$$

$$[K]_{\mathrm{c}}^{\mathrm{uncr}} = \frac{E_{\mathrm{c}}}{1\text{-}\nu_{\mathrm{c}}^2}\begin{bmatrix} 1 & \nu_{\mathrm{c}} & 0 \\ \nu_{\mathrm{c}} & 1 & 0 \\ 0 & 0 & \dfrac{1\text{-}\nu_{\mathrm{c}}}{2} \end{bmatrix} \qquad [K]_{\mathrm{c}}^{\mathrm{cr}} = [T]_{\sigma}^{-1}\begin{bmatrix} 0 or E_{\mathrm{c}}^{'} & 0 & 0 \\ 0 & 0 or E_{\mathrm{c}}^{'} & 0 \\ 0 & 0 & 0 \end{bmatrix}[T]_{\varepsilon} \tag{6}$$

Cracking of concrete infill is judged by comparison between the principal tensile stress and its cracking threshold. Note that, Varma et al. (2011, 2014) recommended that the cracking threshold corresponds to the principal tensile stress of $2\sqrt{f_{\mathrm{c}}^{'}}$ in psi, which accounts for the locked-in shrinkage strains in the concrete and relative slip between the steel faceplate and concrete infill. In addition, the limit of elastic behavior for concrete is set as the minimum (compressive) principal stress of $0.5 f_{\mathrm{c}}^{'}$. The procedure and details of the MBM are discussed in detail in Varma et al. (2011, 2014), Seo et al. (2016), and the basis of the AISC N690s1 (2015) design code.

Validation of MBM

The accuracy of the MBM has been validated by the test data where the DSC walls were subjected to pure in-plane shear or combined in-plane shear and low axial compression (Varma et al. 2014 and Seo et al. 2016). Using the test data from this program, this section evaluates the accuracy of the MBM for predicting the behavior of DSC walls subjected to high axial compression and in-plane shear.

Fig. 9 shows the response of shear force versus shear strain predicted by the MBM, compared with the envelope curve of the cyclic responses of the wall specimens. The MBM model appears to reasonably capture the initial stiffness and the yield strength of the DSC wall specimens. The analytical and experimental curves show some dispersion at the region around the yielding of DSC walls, especially in Fig. 9 (c). This is attributed to the fact that the MBM does not directly account for the slip between the steel faceplates and concrete infill, which may occur when the DSC walls are subjected to high levels of cyclic shear loads. At the yielding of the web faceplates, the estimated angle of the principal tensile strain relative to the horizontal direction was 39°, 34° and 34° for Specimens DSCW1, DSCW2 and DSCW3 respectively, which correlated well with the measured values shown in Fig. 8. Table 4 presents the calculated initial stiffness, yield strength and corresponding shear strain, compared with the test results. In accordance with the MBM, the initial stiffness is estimated by $G_cA_c+G_sA_s$, where G_c and G_s denote the shear modulus of concrete and steel, and A_c and A_s denote the cross-sectional areas of the concrete infill and steel faceplates, respectively. The calculated initial stiffness correlates well with the corresponding experimental result. The calculated value of the yield shear strength is 10% higher than the test value on average, while the calculated value of the yield shear strain is 13% lower than the test value.

Effect of axial force on shear strength

Using the MBM, this section analyzes the influence of axial force on the in-plane yield shear strength of DSC walls. Specimen DSCW2 was considered as a case study for this analysis, and analyzed for a variety of axial tension and compression forces. Fig. 10 shows the relation between in-plane shear strength and axial force ratio. The in-plane shear forces carried by the steel faceplates and by the concrete infill are also plotted in this figure. The axial force ratios in these plots range from -0.5 (compression) to 0.2 (tensile). Note that this interaction curve corresponds to the limit state of the yielding of steel faceplates, except for the axial compressive force ratio of 0.5 which is governed by the minimum (compressive) principal stress of concrete reaching the limiting value of $0.5f'_c$.

The following observations are made from Fig. 10. (1) Under the combined in-plane shear and axial tension, the yield shear strength of the composite wall decreases rapidly along with an increase in the axial tensile force, as the increased tensile stress reduces the shear strengths of both steel faceplates and concrete infill. (2) When ranging from 0 to 0.4, the axial compressive force ratio has limited influence to the in-plane yield shear strength of the composite walls. An increase of axial compressive force leads to a decrease in the shear strength of steel faceplates, while it can increase the shear strength of concrete infill. As a trade-off, the total shear strength of the composite walls remains nearly unchanged. It is notable that the UBC-97 provision limits the axial compressive force ratios to be no greater than 0.35 for ductile structural walls, and EuroCode 8 limits the axial compressive force ratios to be no greater than 0.4 and 0.35 for structural walls with medium and high ductility, respectively.

Effect of steel reinforcement ratio

An increase in the steel reinforcement ratio leads possibly to the increased minimum (compressive) principal stresses in the concrete when the steel faceplates yield. Parametric studies were performed where the geometry and material strength of the walls were identical to those of Specimen DSCW2, while the steel reinforcement ratio and axial force ratio were varied. Based on the MBM analysis, Fig. 11 plots the relationship of in-plane shear strength versus steel reinforcement ratio. Four levels of axial force ratios are considered in this analysis, i.e., n = 0.16, 0.25, 0.30 and 0.40.

Fig. 11 indicates that an increase in the steel reinforcement ratio can effectively improve the in-plane shear strength of DSC walls. Nevertheless, overly large steel reinforcement ratio may result in compressive failure of concrete infill prior to the yielding of faceplates. The balanced reinforcement ratio when the faceplate yields and the principal compressive stress of the concrete reaches 0.7 f_c' are indicated in this figure. Note that 0.7 f_c' is regarded as the effective compressive strength of the concrete in the compressive strut.

This balanced reinforcement ratio is strongly related to the axial force ratio. An increase in the axial force ratio decreases the reinforcement ratio corresponding to the balance point. For example, the balanced steel reinforcement ratio equals to 20% for the axial force ratio of 0.16, while it decreases to 11% for the axial force ratio of 0.30. Corresponding to the axial force ratio of 0.40, which is defined as the upper limit for ductile wall structures by Eurocode 8, the balanced steel reinforcement ratio equals to 7.5%. Therefore, for DSC walls made using normal strength concrete and steel, steel reinforcement ratios of over 7.5% and very high axial load ratios exceeding 0.40 can potentially lead to crushing of the concrete infill prior to yielding of steel faceplates, and thus non-ductile failure modes.

Verification of design equations for shear strength

Overview of design equations in various codes

JEAC-4618 2009 (Japan) and KEPIC-SNG 2010 (S. Korea)

The MBM described earlier forms the basis of the design equations in Japanese code (JEAC-4618 2009) and S. Korean code (KEPIC-SNG 2010) to calculate the in-plane shear strength of DSC walls. The formulas used to calculate the in-plane shear strength (V_n^{MBM}) of composite walls is given by Eq. (7). This in-plane shear strength (V_n^{MBM}) corresponds to the limit state of Von Mises yielding of the steel faceplates, and implicitly includes the contribution of the concrete infill in the principal compression direction and thus the in-plane shear strength.

$$V_n^{MBM} = \frac{K_s + K_{sc}}{\sqrt{3K_s^2 + K_{sc}^2}} A_s f_y \tag{7}$$

$$K_{sc} = \frac{1}{\dfrac{4}{0.7E_c A_c} + \dfrac{2(1\text{-}\nu_s)}{E_s A_s}} \tag{8}$$

$$K_s = G_s A_s \tag{9}$$

In these equations, K_s denotes the plane stress properties of steel faceplates, K_{sc} denotes the orthotropic properties for the 45° cracked concrete, G_s denotes the shear modulus of steel, and A_s and A_c denote the cross-sectional area of steel faceplates and of concrete infill.

AISC N690s1-15 (U.S.)

The design equations in AISC N690s1-15 are also based on the MBM theory. However, the MBM based design strength equation was further simplified for the purpose of design as shown in Eq. (10). In this equation, κ is a calibration factor calculated using Eq. (11). The values of $\bar{\rho}$ in Eq. (11) are calculated using Eq. (12), and they vary from 0.01 to 0.04 for nuclear structures. In these equations, f_c' and f_y denotes the concrete compressive strength and the yield strength of steel in MPa, respectively.

$$V_n^{AISC} = \kappa f_y A_s \tag{10}$$

$$\kappa = 1.11\text{-}5.16\bar{\rho} \le 1.0 \tag{11}$$

$$\bar{\rho} = \frac{1}{83}\frac{f_y A_s}{A_c \sqrt{f_c'}} \tag{12}$$

JGJ 3-2010 (China)

In accordance with JGJ 3-2010, the shear strength of composite walls is calculated based on the superposition method, given by:

$$V_n^{JGJ} = V_s + V_c \tag{13}$$

$$V_s = \frac{0.6}{\lambda - 0.5} f_y A_s \tag{14}$$

$$V_c = \frac{1}{\lambda - 0.5}\left(0.5 f_t b_w h_{w0} + 0.13N\right) \tag{15}$$

The in-plane shear strength of steel plates V_s and the shear strength of concrete infill V_c are estimated using Eq. (14) and (15), respectively. In these equations, f_t denotes the tensile strength of the concrete, b_w denotes the thickness of the concrete infill, h_{w0} denotes the effective depth of the wall section, N denotes the axial compressive force applied to the web wall, and $\lambda = Mh_{w0}/V$ denotes the shear-to-span ratio of the wall. For the cantilever wall specimens, the shear-to-span ratio equals to the wall's aspect ratio. In Eqs. (14) and (15), the lower bound value of λ is limited to 1.5 (i.e., it is assumed to be equal to 1.5 if it is smaller than 1.5). It is important to note that the JGJ 3-2010 equations take directly into account the effect of axial compressive force on the shear strength contribution of the concrete infill.

5.2 Statistical analysis of test data

An experimental database of in-plane shear tests has been assembled by Seo et al. (2016). This paper uses and enhances that database by including data from past tests (Akiyama et al. 1991; Takeda et al. 1995; Takeuchi et al. 1998; Fujita et al. 1998, Ozaki et al. 2001 and 2004 ;

Cao et al. 2013) and from this test program. Fig. 12 shows the comparison between the calculated values per the design equations and the test results. A total of 42 test specimens are considered, of which the steel reinforcement ratio varies from 1.3 to 6.4%, and the axial compressive force ratio varies from zero to 0.31.

Fig. 12 indicates JEAC, KEPIC, AISC and JGJ code equations provide reasonable and conservative assessment of the in-plane shear strength of DSC walls. Most of the calculated values of V_n according to these equations are lower than the test values V_{Test}. The mean value of the ratio V_{Test}/V_n varies slightly from 1.29 to 1.36 for various codes. The standard deviation of the ratio V_{Test}/V_n is approximately 0.23.

Conclusions

This paper presented the results from a series of quasi-static cyclic tests and numerical analysis (conducted using a mechanics based model) to evaluate: (i) the cyclic in-plane shear behavior of double skin composite (DSC) walls used in high-rise buildings, and (ii) the influence of higher steel reinforcement ratios and axial force ratios on the in-plane shear behavior of DSC walls. The following conclusions were drawn from this study:

(1) The DSC wall specimens failed in a shear mode, induced by yielding followed by local buckling of steel faceplates and crushing of concrete infill. The DSC wall specimens had stable hysteretic loops even when subjected to high axial force ratio and large cyclic shear deformations, as the steel faceplates could undergo cyclic yielding while preventing spalling of the concrete infill.

(2) Increasing the axial ratio from 0.16 to 0.30 had limited influence to the shear strength of the DSC walls, but it resulted in approximately 20% reduction in the shear deformation

capacity for the tested specimens.

(3) The DSC specimen with vertical stiffeners and tie plates connecting the two faceplates had larger shear deformation capacity than the specimens with headed shear studs and tie bars as connectors. The former had the ultimate shear strain reaching approximately 3%.

(4) Parametric studies conducted using the mechanics based model (MBM) indicate that the axial compressive force ratio ranging from 0 to 0.40 has limited influence to the in-plane yield shear strength of the DSC walls. However, higher reinforcement ratios of greater than 7.5% and axial load ratios of greater than 0.40 may lead to concrete crushing limit states governing before steel yielding, and thus non-ductile failure modes for the DSC walls.

(5) Analysis of the test results of 42 DSC wall specimens from past tests and from this program indicates that the design equations of JEAC-4618 2009 (Japan), KEPIC-SNG 2010 (S. Korea), AISC N690s1-15 (U.S.) and JGJ 3-2010 (China) can provide reasonable and conservative estimates of the shear strength of DSC walls. The mean value of the ratio of the experimental shear strength over those calculated strength using different design code equations varies slightly from 1.29 to 1.36.

Acknowledgments

The work presented in this paper was sponsored by National Key Technology R&D Program of China (Grant No. 2012BAJ07B01) and by the National Natural Science Foundation of China (Grant No. 51261120377). Partial funding was provided by Purdue University to complete the manuscript for the paper. The writers wish to express their sincere gratitude to the sponsors.

References

Akiyama, H., Sekimoto, H., Fukihara, M., and Hara, K. (1991). “A compression and shear loading test of concrete filled steel bearing wall.” *Transaction of the 11th International Conference on Structural Mechanics in Reactor Technology*, Tokyo, Japan, H: 323-328.

AISC (American Institute of Steel Construction). (2010). “Seismic provisions for structural steel buildings.” *ANSI/AISC 341-10*, Chicago.

AISC (American Institute of Steel Construction). (2015). “Specification for safety-related steel structures for nuclear facilities including supplement no. 1.” *AISC N690s1-15*, Chicago.

Alzeni, Y., and Bruneau, M. (2014). “Cyclic inelastic in-plane behavior of concrete filled steel sandwich panel walls.” *Proceedings of Tenth U.S. National Conference on Earthquake Engineering*. Anchorage, USA, Paper No. 000420.

Bruneau, M., Varma, A.H., and Hooper, J. (2016). “Composite plate shear walls--concrete filled (C-PSW/CF)”. *2016 NASCC: The Steel Conference Proceedings*. Orlando, USA, Online at http://media.aisc.org/NASCC2016/N71B.mp4

CMC (China Ministry of Construction). (2010). “Code for design of concrete structures.” *GB 50010-2010*, Beijing.

CMC (China Ministry of Construction). (2010). “Technical specification for concrete structures of tall building .” *JGJ 3-2011*, Beijing. (in Chinese).

Cao, W., Yu, C., Dong, H., Qiao, Q., Han, L., and Zhang, Y. (2013). “Experimental study on performance of composite shear walls with double steel plate under different constructions.” *J. Build. Struct.*, 34(Supplement 1), 186-191 (in Chinese).

Ding, Z., Jiang, H., Zeng, J., Zhang, H., and Du, G. (2011). “An innovative application of

SCS composite wall: Structural design of Yancheng TV Tower." *Build. Struct.*, 41(12), 87-91 (in Chinese).

ECS (European Committee for Standardisation). (2003). "Design of structures for earthquake resistance. Part 1: general rules, seismic actions and rules for buildings." *Eurocode 8*, Brussels.

Eom, T. S., Park, H. G., Lee, C. H., Kim, J. H., and Chang, I. H. (2009). "Behavior of double skin composite wall subjected to in-plane cyclic loading." *J. Struct. Eng.*, 135(10), 1239-1249.

Fujita, T., Funakoshi, A., Akita, S., Hayashi, N., Matsuo, I., and Yamaya, H. (1998). "Experimental study on a concrete filled steel structure Part. 16 Bending shear tests (effect of bending strength)." *Summaries of Technical Papers of Annual Meeting*, Architectural Institute of Japan: 1125-1126 (in Japanese).

ICBO (International Council of Building Officials). (1997). "Uniform Building Code", *UBC*, Whittier.

JEAC (Japanese Electric Association Nuclear Standards Committee). (2009). "Technical code for seismic design of steel plate reinforced concrete structures: Buildings and structures." *JEAC-4618*, Tokyo (in Japanese).

Ji, X., Jia, X., and Qian, J. (2015). "Experimental study on shear behavior of steel-plate composite shear walls." *J. Build. Struct.*, 36(11): 46-55 (in Chinese).

Ji, X., Jiang, F., and Qian, J. (2013). "Seismic behbavior of steel tube-double steel plate-concrete composite walls: Experimental tests." *J. Constr. Steel. Res.*, 86(7), 17-30.

KEPIC-SNG. (2010). "Specification for safety-related steel plate concrete structures for nuclear facilities." Board of KEPIC Policy, Structural Committee, Korea Electric Association.

Kurt, E.G., Varma, A. H., Booth, P. N., Whittaker, A.S. (2016). "In-plane behavior and design of rectangular SC wall piers without boundary element." *J. Struct. Eng.*, 142(6), 10.1061/(ASCE)ST.1943-541X.0001481, 04016026.

Liew, J. Y. R., Yan, J. B., and Huang, Z. Y. (2015). "Steel-concrete-steel sandwich composite structures – the current state of the art." Proc, *11th International Conference on Advances in Steel and Composite Structures*, Association for Steel-Concrete Composite Structures, Beijing.

Nie, J., Hu, H., Fan, J., Tao, M., Li, S., and Liu, F. (2013). "Experimental study on seismic behavior of high-strength concrete filled double-steel-plate composite walls." *J. Constr. Steel. Res.*, 88(9), 206-219.

Ozaki, M., Akita, S., Niwa, N., Matsuo, I., and Usami, S. (2001). "Study on steel plate reinforced concrete bearing wall for nuclear power plants Part I: shear and bending loading tests of SC walls." *Transaction of the 16th International Conference on Structural Mechanics in Reactor Technology*, Washington DC , Paper ID: 1554.

Ozaki, M., Akita, S., Niwa, N., Osuga, H., Nakayama, T., and Adachi, N. (2004). "Study on steel plate reinforced concrete panels subjected to cyclic in-plane shear." *Nucl. Eng. Des.*, 228, 225-244.

Sener, K.C., and Varma, A.H. (2014). "Steel-plate composite walls: experimental database and design for out-of-plane shear." *J. of Constr. Steel. Res.*, 100, 197-210.

Shirali, M. N. (2002). "Seismic resistance of a hybrid shearwall system." Ph.D. Dissertation, *Darmstadt University of Technology*, Germany.

Seo, J., Varma, A. H., Sener, K., and Ayhan, D. (2016). “Steel-plate composite (SC) wall: In-plane shear behavior, database, and design.” *J. Constr. Steel. Res.*, 119, 202-215.

Takeda, T., Yamaguchi, T., Nakayama, T., Akiyama, K., and Kato, Y. (1995). “Experimental study on shear characteristics of a concrete filled steel plate wall.” *Transaction of the 13th International Conference on Structural Mechanics in Reactor Technology*, Porto Alegre, Brazil, H03: 21-26.

Takeuchi, M., Narikawa, M., Matsuo, I., Hara, K., and Usami, S. (1998). “Study on a concrete filled structure for nuclear power plants.” *Nucl. Eng. Des.*, 179, 209-223.

Varma, A. H., Zhang, K., Chi, H., Booth, P., and Baker, T. (2011) “In-plane shear behavior of SC composite walls: theory vs. experiment.” *Proceedings of the 21st IASMiRT Conference. SMiRT 21*, New Delhi, India.

Varma, A. H., Malushte, S. R., Sener, K. C., Lai, Z.C. (2014). “Steel-plate composite walls for safety related nuclear facilities: Design for in-plane forces and out-of-plane moments.” *Nucl. Eng. Des.*, 269, 240-249.

Zhang, K., Varma, A. H., Malushte, S. R., Gallocher, S. (2014). “Effect of shear connectors on local buckling and composite action in steel concrete composite walls.” *Nucl. Eng. Des.*, 269, 231-239.

Table 1. Design parameters of wall specimens

Spec. no.	Stud/stiffener spacing (mm)	Tie bar/plate spacing (mm)	Faceplate slenderness ratio	Reinforcement ratio $2t_p/T$	Total axial force (kN)	Axial force ratio n
DSCW1	100	200	25	6.4%	1389	0.16
DSCW2	100	200	25	6.4%	2779	0.31
DSCW3	150	80	37.5	6.4%	2779	0.31

Table 2. Material properties of steel

Plate thickness t_p (mm)	Yield strength $f_{y,t}$ (MPa)	Ultimate strength $f_{u,t}$ (Mpa)	Elongation δ (%)
4	341.1	496.3	28.9
8	302.1	450.8	37.3

Table 3. Shear strength and deformation capacity of specimens

Spec. no.	Yield load V_y (kN)	Yield shear strain γ_y (%)	Peak load V_p (kN)	Peak shear strain γ_p /%	Ultimate shear strain γ_u /%	Ductility ratio μ_γ
DSCW1	1878	0.27	2212	0.93	1.54	5.7
DSCW2	1797	0.22	2306	0.68	1.12	5.1
DSCW3	1735	0.26	2387	1.25	3.09	11.9

Table 4. Comparison between MBM analytical value and experimental results

Spec. no.	Initial stiffness		Yield shear strain		Yield shear strength	
	K^{test} ($\times 10^6$ kN)	K^{calu} ($\times 10^6$ kN)	γ_y^{test} (%)	γ_y^{calu} (%)	V_y^{test} (kN)	V_y^{calu} (kN)
DSCW1	1.38	1.49	0.27	0.23	1878	1939
DSCW2	1.48	1.48	0.22	0.23	1797	1963
DSCW3	1.41	1.48	0.26	0.23	1735	1963

(a) Yancheng television tower (b) Site construction

Fig. 1. Photographs of double-skin composite wall construction

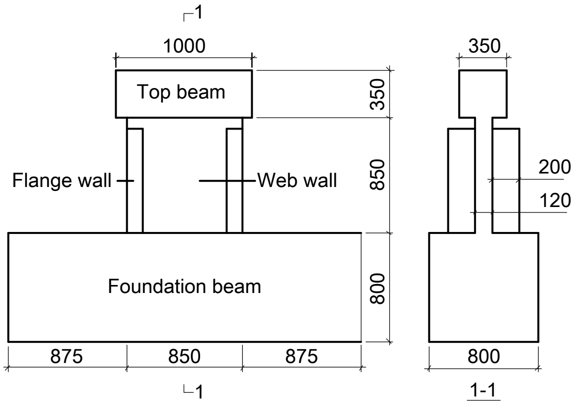

(a) Overall geometry dimension

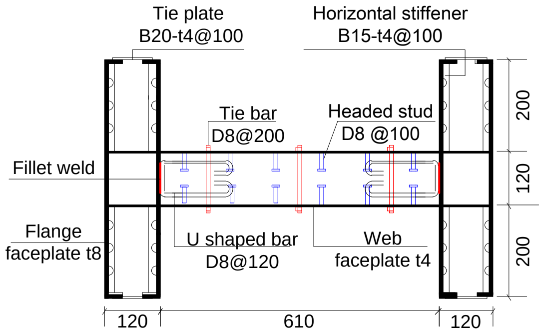

(b) Cross section

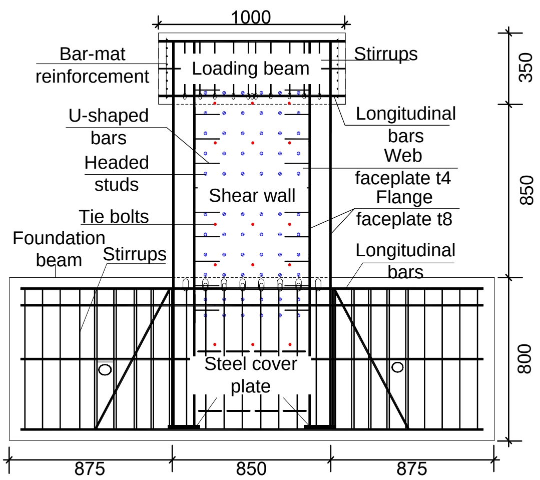

(c) Elevation view

Fig. 2. Geometry and reinforcement of Specimens DSCW1 & DSCW2 (unit: mm)

555

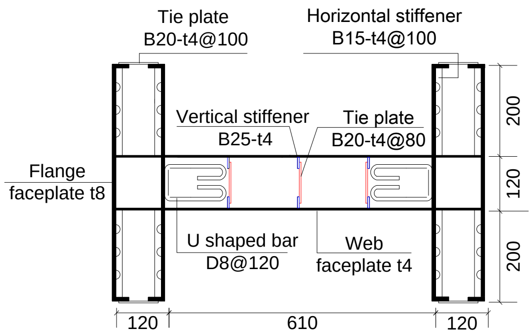

(a) Cross section

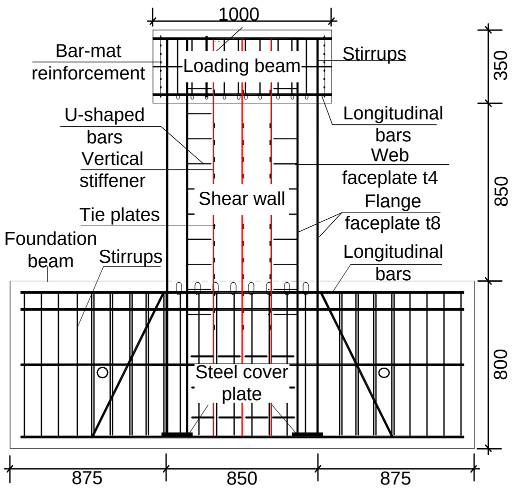

(b) Elevation view

Fig. 3. Geometry and reinforcement of Specimen DSCW3 (unit: mm)

556

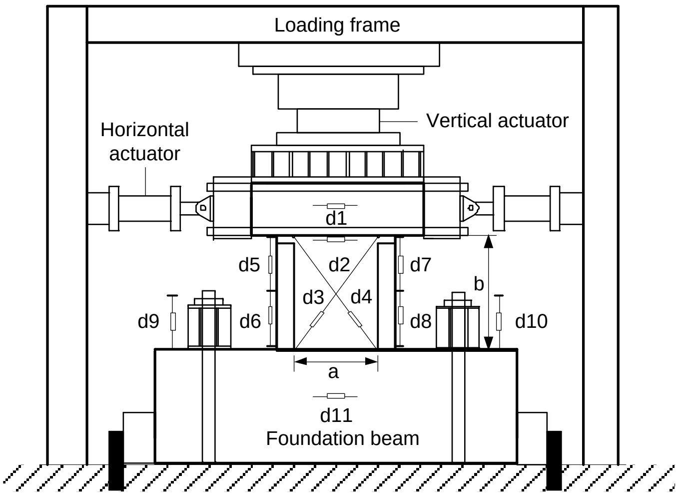

(a) Sketch of test setup

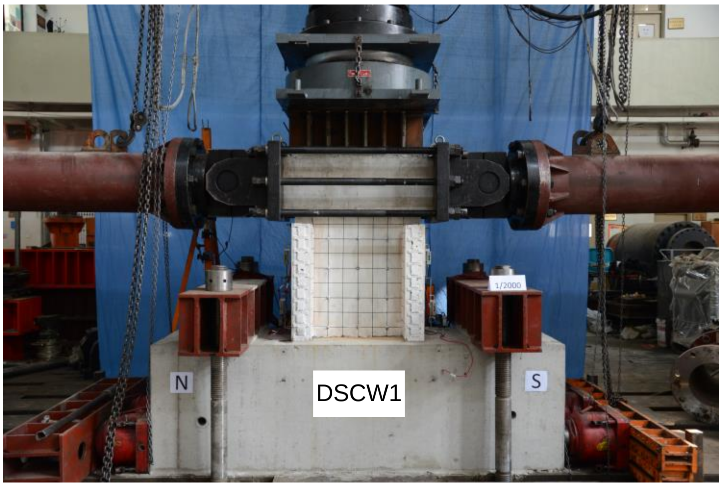

(b) Photograph of test setup

Fig.4. Test setup

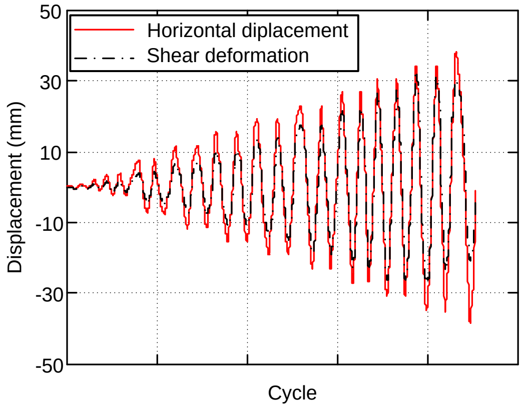

Fig. 5. Shear deformation versus total deformation for Specimen DSCW3

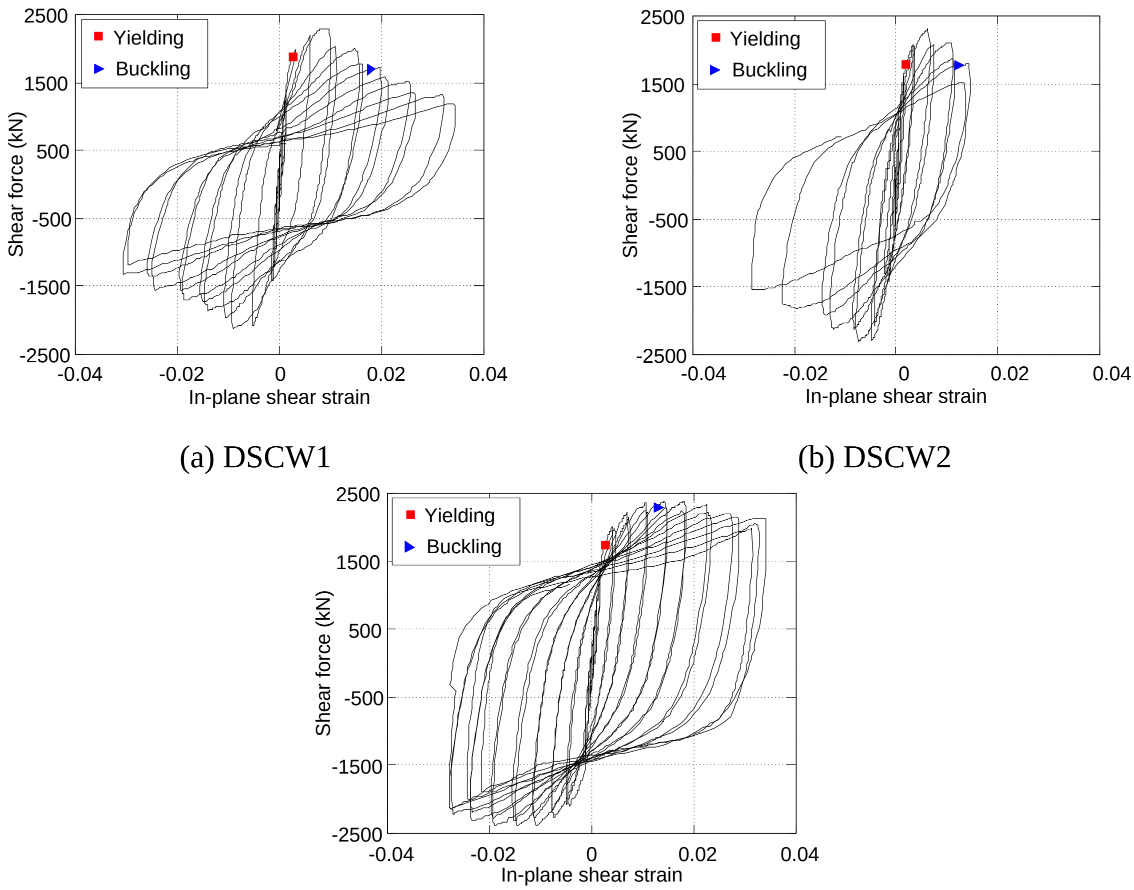

(a) DSCW1

(b) DSCW2

(c) DSCW3

Fig. 6. Hysteretic loops of lateral force versus in-plane shear strain of specimens.

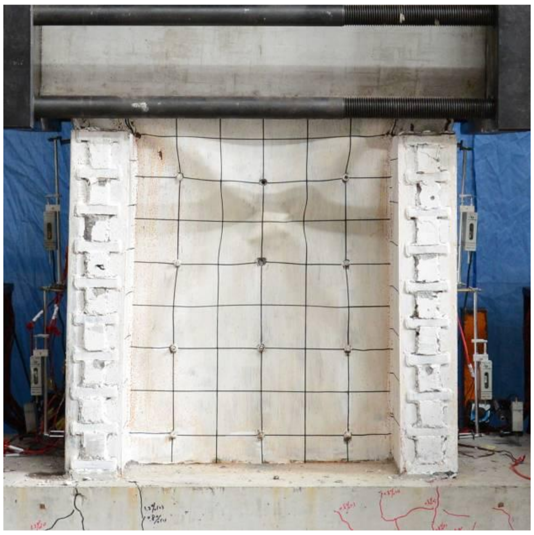

(a) Specimen DSCW1

(b) Specimen DSCW2

(c) Specimen DSCW3

Fig. 7. Failure photographs of the wall specimens

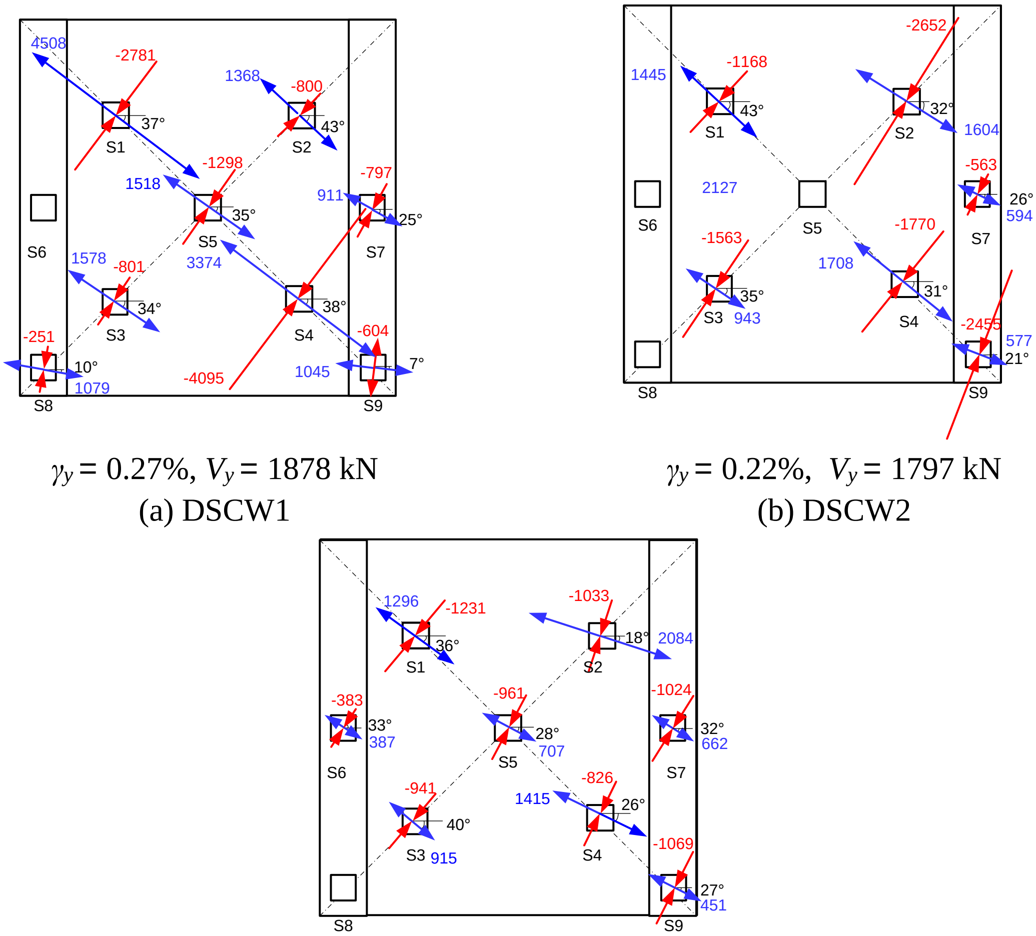

$\gamma_y = 0.27\%$, $V_y = 1878$ kN

(a) DSCW1

$\gamma_y = 0.22\%$, $V_y = 1797$ kN

(b) DSCW2

$\gamma_y = 0.26\%$, $V_y = 1735$ kN

(c) DSCW3

Fig. 8. Principal strains of steel faceplates.

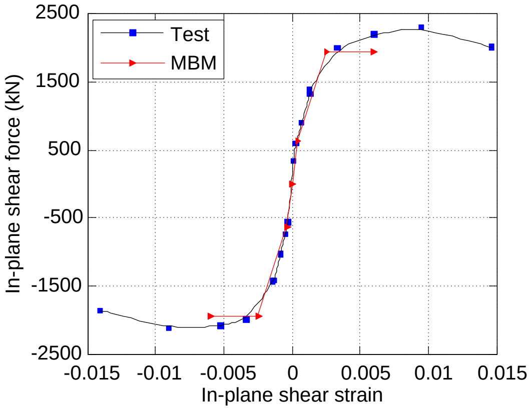

(a) DSCW1

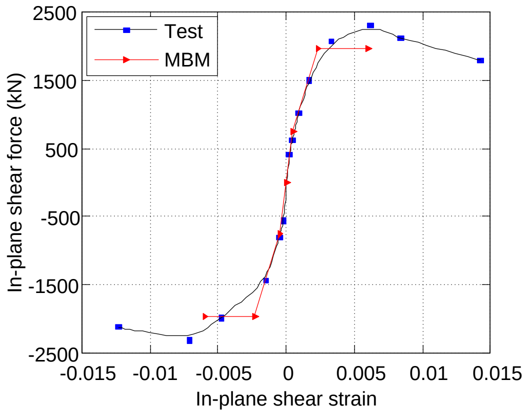

(b) DSCW2

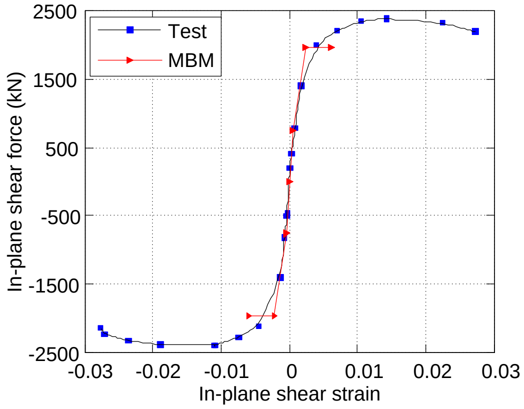

(c) DSCW3

Fig. 9. Comparison of experimental and analytical in-plane shear force versus shear strain response

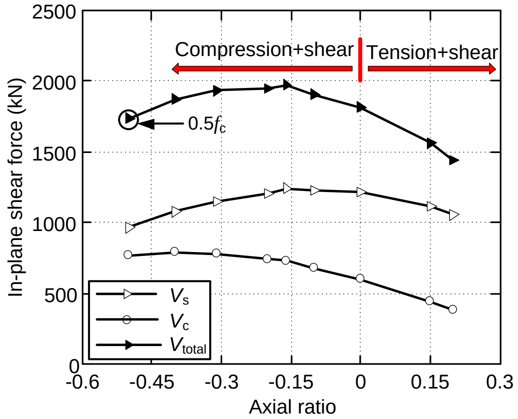

Fig. 10. The relationship of shear yielding strength with the axial ratio

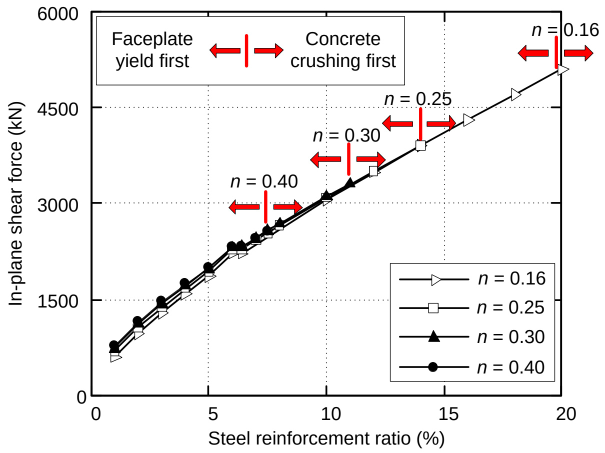

Fig. 11. Effect of steel reinforcement ratio

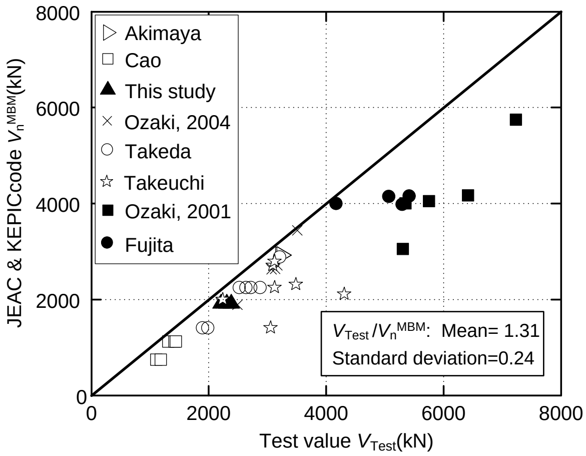

(a) JEAC-4618 2009 (Japan) and KEPIC-SNG 2010 (S. Korea)

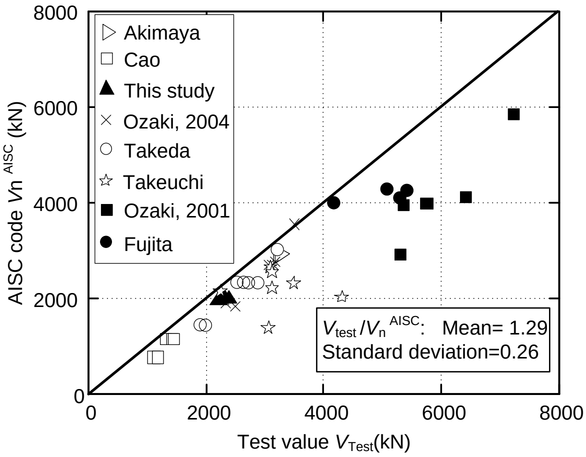

(b) AISC N690s1-15 (U.S.)

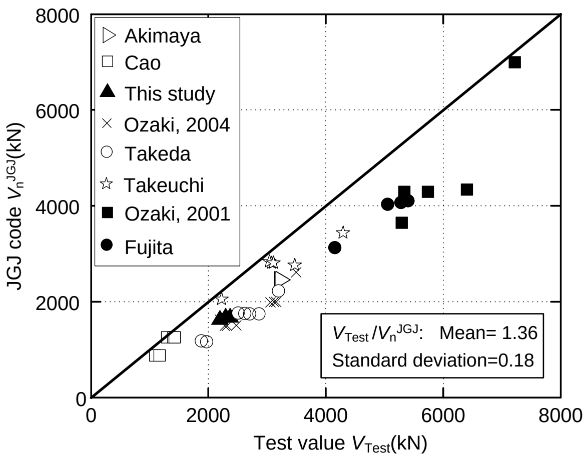

(c) JGJ 3-2010 (China)

Fig. 12. Verification for design formulas of shear strength